Computational Modeling of Hybrid Graphene/Quantum Dot Photodetectors

Hassan Imran and Saqib Iqbal
Department of Electrical Engineering
School of Science and Engineering
LUMS, Lahore, 54792, Pakistan
Email: 15060064@lums.edu.pk;
15060005@lums.edu.pk

Amina Farooq
Department of Physics
School of Science and Engineering
LUMS, Lahore, 54792, Pakistan
Email: 16120011@lums.edu.pk

Nauman Z. Butt
Department of Electrical Engineering
School of Science and Engineering
LUMS, Lahore, 54792, Pakistan
Email: nauman.butt@lums.edu.pk

***Abstract*—Ultrahigh sensitive phototransistors featuring a hybrid channel of graphene and a photoabsorbing nanomaterial which is backgated through a substrate have demonstrated photoresponsivity (in the range of $10^1 - 10^7$ A/W). Although remarkable sensitivity has been validated on a variety of photoabsorbers such as quantum dots, perovskites, and, dyes, *etc.*, basic physical principles and design parameters have not been well understood using a self-consistent model. In particular, the relative contribution of two distinct mechanisms for graphene photoconduction: (i) carrier injection from nanomaterial, and, (ii) photo-induced field effect from the substrate, is unclear. Here, we use self-consistent numerical simulations to quantify these effects and show that both mechanisms can have an equivalent effect when the substrate is undoped. As the substrate doping increases, the latter process rapidly falls off due to charge screening. We further explore the effect of source/drain/gate metal workfunction, substrate doping, and, carrier lifetimes and propose optimizations for performance enhancement.**

I. INTRODUCTION

A large number of applications require highly sensitive photodetectors that can sense light from the ultraviolet (UV) to the infrared (IR) range [1]. Ideally, these photodetectors should have a good compatibility with CMOS platforms for monolithic integration to provide high density, high throughput and cost effective manufacturing processes [2]. Graphene [3], quantum dots (QDs) [4], perovskite [5] *etc.* are easy to integrate with silicon and can be tuned to offer a low cost and highly sensitive photodetection in a broad range of wavelength. During past few years, photodetectors made of these materials have demonstrated very high quantum efficiency *i.e.* the number of photogenerated carriers per incident photon, low noise, high photoresponsivity and high gain.

A remarkably high performance in hybrid graphene photodetecrors compared to that of the conventional photodetectors rely on unique properties in particular, its high carrier mobility and its atomically thin profile [6]. The high carrier mobility in graphene allows ultrafast conversion of photogenerated carriers into electrical current or voltage. Yet, thin sheet of zero bandgap graphene inhibits efficient optical absorption in UV and visible spectrum. To counter the low optical absorption in graphene, , highly sensitive graphene based photodetectors have been realized with some emerging and cost effective materials like QDs [7], perovskite [8], dyes [9], and other 2–D materials [10] *etc.* and have exhibited a high photoresponsivity.

In hybrid graphene phototransistor, light is absorbed in a nanomaterial (perovskite, QD, dye, *etc.*) which makes a Schottky contact with graphene channel from top. The channel is contacted with source/drain metals and is modulated through a backgate under substrate. The photogenerated carriers are separated due to energy barriers at graphene/metal and graphene/nanomaterial junctions under an applied backgate voltage. Photocurrent arises due to electrostatic doping of graphene either due to direct injection of photogenerated carriers from nanomaterial into graphene or due to the electrostatic field effect of the photogenerated carriers in substrate. Photoresistance of graphene ($R_g = 1/q\mu\Delta Q$), where q is the charge on electron, μ is the mobility of charge carriers, ΔQ is the change in carrier density (doping) of graphene, defines photoresponse. In the existing models, ΔQ is calculated based on the carrier transport in Schottky diode formed between graphene and nanomaterial. The carrier transport and current continuity along the graphene channel is generally ignored due to which important effects such as carrier trapping/accumulation inside the channel are not incorporated.

Here, we include the effect of carrier transport along the channel and show that lateral potential profile along source/drain junctions can significantly modulate ΔQ. We also incorporate the electrostatic effect of the photogenerated carriers in substrate to highlight its relative contribution to the photoresponse.. In addition, we explore the effect of incident photon power on device photoresponsivity, the effects of carrier lifetime in quantum dots and substrate, the workfunction of source/drain metal and the workfunction of backgate metal with the substrate. Since all of these parameters could vary as a function of deposition/process methods *etc.*, their role on the device characteristics needs to be well assessed.

This paper is divided into four sections. Section II describes the modeling approach. Section III discusses the results and the conclusions are provided in Section IV.

II. MODELING APPROACH

A three dimensional (3–D) schematic and 2–D cross section of the device modeled in this work are shown in Fig. 1(a)

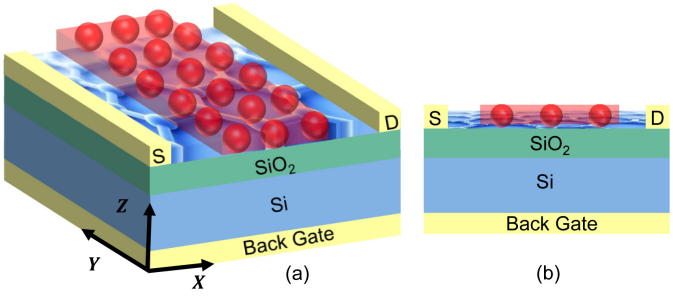

Fig. 1. (a) Three dimensional (3–D) illustration of the hybrid graphene/quantum dot photodetector modeled in this work. (b) 2–D cross section of the hybrid photodetector. A single layer graphene forms the channel between source and drain which is backgated through silicon (Si) substrate. Qunatum Dot (QD) layer is used as photoabsorber.

and 1(b) respectively. The device consists of a single layer graphene which forms the channel between source and drain which is backgated through silicon (Si) substrate, while QD layer is used as photoabsorbing material. The light is incident on QD and a photon flux is transferred into graphene and moves into source and drain producing a photogenerated current (I_{photo}). The device is simulated using a semi-classical simulation tool Padre [11] for the first order evaluation of various effects. It solves the Poisson equation and carrier

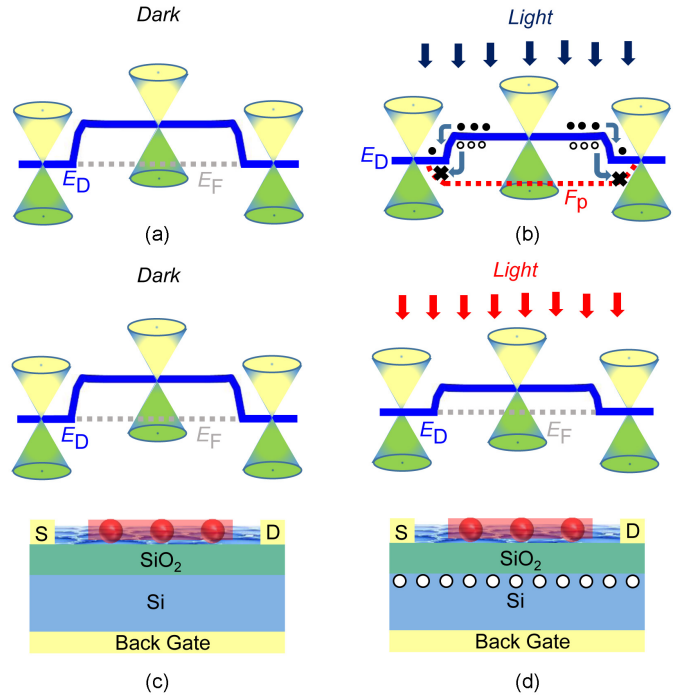

Fig. 2. (a,b) The lateral potential of graphene channel under dark and illumination for incident photon of smaller wavelength (λ). Photogenerated carriers are trapped inside graphene due to the energy trap created inside graphene channel. Due to charge trapping, graphene potential and resistance (R_g) are changed under illumination. (c,d) The lateral potential of graphene channel under dark and illumination for incident photon of higher λ when light is absorbed in Si substrate. The photogenerated carriers accumulated at Si/SiO_2 interface and modulated graphene potential and R_g.

continuity equations self-consistently assuming drift-diffusion transport. Poisson equation is given by:

$$\bigtriangledown^2 V(x) = \frac{q}{\epsilon}\left[N_D - N_A + p(x) - n(x)\right] \tag{1}$$

where $V(x)$ is the electrostatic potential, ϵ is the the permittivity of the absorber, N_D (N_A) are donor (acceptor) doping density, $n(x)$ and $p(x)$ are position dependent electron and hole concentration respectively. The continuity equation for electrons (holes) is given by:

$$\frac{\partial n(p)}{\partial t} = \frac{\overset{+}{(-)}1}{q} \bigtriangledown \cdot J_{n(p)} + G(x) - R(x) \tag{2}$$

where $J_{n(p)}$ is electron (hole) current density, $G(x)$ & $R(x)$ are position dependent carrier generation and recombination rates respectively. The drift-diffusion equation for electrons (holes) is given by:

$$J_{n(p)} = qn(p)\mu_{n(p)}\frac{dV(x)}{dx} \overset{+}{(-)} qD_{n(p)}\frac{dn(p)}{dx} \tag{3}$$

where $\mu_{n(p)}$ is the mobility of electrons (holes) and $D_{n(p)}$ is the diffusion constant for electrons (holes) respectively. $G(x)$ inside the absorber is implemented using Lambert-Beer Law and given by [12]:

$$G(x) = \alpha G_0 e^{-\alpha x} \tag{4}$$

where G_0 is the photogeneration at front surface. α is the absorption coefficient of the absorber and x is the position inside the absorber.

Recombination models include radiative, Shockley-Reed-Hall and Auger processes. A 2 nm graphene layer is implemented as an ultrathin semiconductor with mobility matching experimental values for graphene. The QD layer is 80 nm implemented in an effective medium approximation assuming an average mobility, bandgap, and, dielectric constant for the QD medium [13]. The device under observation is illuminated with both high and low energy incident photons in order to investigate the relative contribution of QD and substrate on device photoresponsivity (R).

The basic working principle of the device for incident photons of smaller wavelength (λ) under dark and illumination is shown in Fig. 2(a) and 2(b) respectively. Due to large α of QD for high energy photons, the photogeneration takes place inside QD layer and the photogenerated carriers are transferred into graphene. Due to a built-in electric field, one type of carriers flow towards source and drain while the other type of carriers are trapped inside graphene making it either n-type or p-type depending upon the type of trapped carriers. The accumulation of trapped carriers inside graphene channel modulates R_g. Due to the change in R_g under dark and light, I_{photo} flows between source and drain for an applied source/drain voltage (V_{ds}).

The basic working principle of the device for incident photons of larger λ under dark and illumination is shown in Fig. 2(c) and 2(d) respectively. Due to small α of QD for low energy photons and small QD layer thickness, most

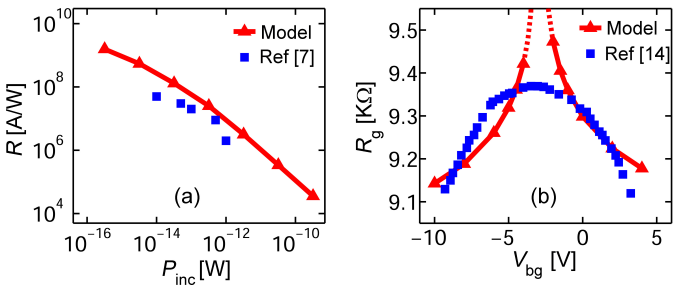

Fig. 3. (a) Photoresponsivity (R) as a function of incident photon power (P_{inc}). The hybrid photodetector exhibits a high R ($\approx 10^9$A/W) for P_{inc} as low as 10^{-16} W. The solid line shows the power law fit ($R \propto P_{\text{inc}}^{\beta}$) for the simulated data with $\beta = -0.83$. (b) Experimental backgate voltage (V_{bg}) modulation of graphene resistance ($R_{\text{g}} - V_{\text{bg}}$) is compared with the simulated $R_{\text{g}} - V_{\text{bg}}$. The Fig. shows a good match with the experimental ambipolar symmetric $R_{\text{g}} - V_{\text{bg}}$ characteristics.

of the photogeneration takes place inside Si and the photogenerated carriers move towards their respective contacts under an applied backgate voltage (V_{bg}). Due to a thick SiO_2 layer, one type of carriers start accumulating at Si/SiO_2 interface. The presence of space charge density at Si/SiO_2 interface electrostatically dope graphene either n-type or p-type depending upon the type of space charge. The doping of graphene defines the number of carriers density and is responsible for R_{g}. Due to modulation in R_{g} under dark and illumination, I_{photo} flows between source and drain for and applied V_{ds}.

III. RESULTS AND DISCUSSION

R of the hybrid photodetector as a function of incident photon power (P_{inc}) is shown in Fig. 3(a). The hybrid graphene/quantum dot photodetector exhibits a high R ($\approx 10^9$ A/W) for P_{inc} as low as 10^{-16} W. The solid line shows the power law fit ($R \propto P_{\text{inc}}^{\beta}$) for the simulated data with $\beta = -0.83$. The Fig. shows a good match of R vs. P_{inc} with the experimental data of [7].

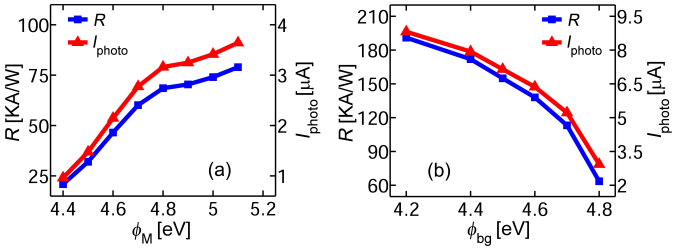

Fig. 4. (a) Effect of front (source/drain) metal workfunction (ϕ_{M}) on R and photogenerated current (I_{photo} . The higher ϕ_{M} increases the Schottky barrier (ϕ_{SB}) between graphene and metal due to which more photogenerated carriers for a given V_{bg} are trapped inside graphene to modulate R_{g}. The modulation in R_{g} under dark and light results in R and I_{photo}. (b) Effect of backgate metal workfunction (ϕ_{bg}) on R and I_{photo}. The lower ϕ_{bg} increases ϕ_{SB} between undope Si and backgate due to which more photogenerated carriers accumulated at Si/SiO_2 interface to modulate R_{g} which results in R and I_{photo}.

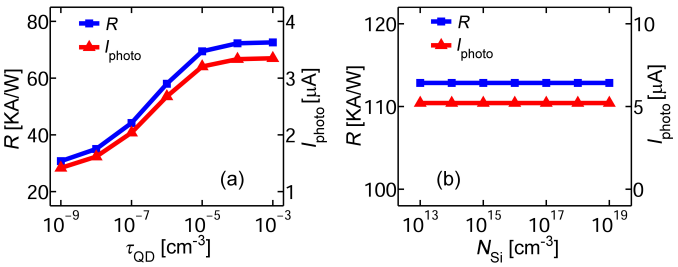

Fig. 5. (a) Effect of carrier lifetime in QD (τ_{QD}) and (b) substrate doping (N_{Si}) on R and I_{photo} for $\lambda = 600$ nm when most of the photogeneration takes place inside QD. (a) For higher τ_{QD}, more photogenerated carreris can transfer into graphene and modulate R_{g} and ultimately R and I_{photo}. (b) For smaller λ, R and I_{photo} are independent of N_{Si}.

Fig. 3(b) represents R_{g} as a function of V_{bg} for the hybrid photodetector. For small V_{bg}, graphene channel potentially remains undoped and R_{g} is high due to the fact that density of states (DOS) is small near the Dirac point (E_{D}) of graphene. As V_{bg} is increased in either direction, the potential of graphene varies making graphene either n-type or p-type. Due to doping of graphene, the DOS is increased away from E_{D} and R_{g} becomes small. Due to change in R_{g}, I_{photo} flows between source and drain for an applied V_{DS}. The symbols shows the experimental data of ambipolar symmetrical $R_{\text{g}} - V_{\text{bg}}$ characteristics of [14].

The effect of front (source/drain) metal workfunction (ϕ_{M}) on R and I_{photo} is shown in Fig. 4(a) for a fixed V_{bg}. Due to difference in metal and graphene workfunctions, a Schottky contact is formed between metal and graphene and electrons can either transfer into graphene from metal or into metal from graphene making graphene n-type or p-type respectively underneath the metal contact. The graphene channel far away from metal remains undoped. More the mismatch between the workfunctions, higher Schottky barrier is formed between metal and graphene. The Fig. shows that for higher metal workfunction (ϕ_{M}), higher R and I_{photo} is achieved due to formation of a higher Schottky barrier between front metal and graphene.

The effect of backgate metal workfunction (ϕ_{bg}) on R and

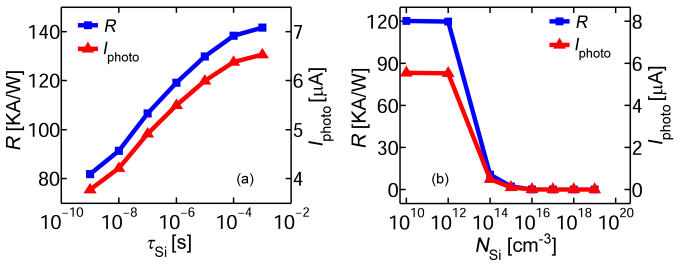

Fig. 6. (a) Effect of carrier lifetime in Si (τ_{Si}) (b) N_{Si} on R and I_{photo} for higher λ when most of the photogeneration takes place inside Si. (a) For higher τ_{Si}, more photogenerated carriers accumulate at Si/SiO_2 interface to modulate R_{g} which results in R and I_{photo}. (b) R and I_{photo} drop drastically even for lightly doped Si, illustrating intrinsic Si is used for $\lambda = 900$ nm to achieve greater R.

I_{photo} is shown in Fig. 4(b). The graphene channel potential under top metal is fixed at the potential of the metal. On the other hand, the graphene channel potential far from the top metal is floating and can be modulated through V_{bg}. The Schottky barrier (ϕ_{SB}) formed between Si and backgate determines the modulation of graphene channel with the application of V_{bg}. The Schottky barrier between Si and backgate is due to difference in workfunctions of Si and backgate metal. Therefore, as ϕ_{bg} is increased, ϕ_{SB} is decreased with undoped silicon. For smaller ϕ_{SB}, less number of photogenerated carriers accumulate at Si/SiO_2 interface under illumination. Due to this phenomenon, the modulation in R_{g} becomes small and R and I_{photo} drops significantly.

The effect of minority carrier lifetime in QD (τ_{QD}) on R and I_{photo} is shown in Fig. 5(a) for incident photons of $\lambda = 600$ nm when light is absorbed in QD layer. For higher τ_{QD}, more photogenerated carriers are trapped inside graphene due to presence of energy trap inside graphene channel for a given V_{bg}. The large number of accumulated carriers inside graphene channel under illumination modulate R_{g}. The higher modulation of R_{g} results in higher R and I_{photo} for a given P_{inc}. It is clear form the Fig. that for higher R and I_{photo}, large τ_{QD} is required.

The effect of substrate doping (N_{Si}) on R and I_{photo} is shown in Fig. 5(b) for incident photons of shorter λ. The electrostatic field effect of substrate doping on R_{g} is negligible due to absence of any photogenerated carriers inside Si. Therefore, both R and I_{photo} are independent of N_{Si}.

The effect of minority carrier lifetime in silicon (τ_{Si}) on R and I_{photo} is shown in Fig. 6(a) for incident photons of $\lambda = 900$ nm when photogeneration takes place inside Si. The photogenerated carriers accumulate at Si/SiO_2 interface and the potential of graphene is modulated due to the photo-induced field effect. For higher τ_{Si}, more carriers accumulate at Si/SiO_2 interface and modulation in graphene potential and R_{g} is higher. Hence, high R and I_{photo} are achieved for higher τ_{Si}.

The effect of substrate doping (N_{Si}) on R and I_{photo} is shown in Fig. 6(b) for incident photons of larger λ. The electrostatic field effect rapidly falls as substrate doping is increased due to charge screening. Unlike case of smaller λ, the Fig. shows that intrinsic substrate is require to achieve higher R and I_{photo} for this case.

IV. CONCLUSIONS

In conclusion, a self-consistent computational model is developed for hybrid graphene/quantum dot photodetectors for the first time. We incorporate the carrier injection from the nanomaterial, lateral transport along the channel, and, the electrostatic effect induced by substrate photogeneration to quantify their relative contributions to the photoresponse. The hybrid photodetector exhibits a high responsivity ($R \approx 10^9$ A/W) for P_{inc} as low as 10^{-16} W. Moreover, the effect of source/drain metal workfunction is also established. A higher ϕ_{M} makes a larger Schottky barrier with graphene and higher R and I_{photo} is achieved. We further investigated the effect of backgate metal workfunction. Smaller the ϕ_{bg}, higher will be R and I_{photo} due to smaller ϕ_{SB} with undoped Si. In addition, we explored the role of QD and substrate for incident photons of different wavelengths. For incident photons of shorter wavelength, light is absorbed in QD layer, and higher carrier lifetime in QD is required to achieve higher R and I_{photo}. While electrostatic effect of substrate doping is negligible for this case. On the other hand, for incident photons of higher wavelength, light is absorbed in silicon, and higher carrier lifetime in silicon is required to achieve higher R and I_{photo}. But unlike previous case, both R and I_{photo} fall off drastically even for lightly doped silicon substrate due to charge screening. Hence, a careful design of quantum dot layer, silicon substrate and source/drain/backgate metal workfunction could is required for highly sensitive hybrid graphene/quantum dot photodetector.

ACKNOWLEDGMENT

The authors would like to thank W. Ahmad, U. B. Qasim and M. Awais for fruitful discussions.

REFERENCES

[1] C. Downs and T. E. Vandervelde, "Progress in infrared photodetectors since 2000," *Sensors*, vol. 13, no. 4, pp. 5054–5098, 2013.

[2] I. Nikitskiy, S. Goossens, D. Kufer, T. Lasanta, G. Navickaite, F. H. Koppens, and G. Konstantatos, "Integrating an electrically active colloidal quantum dot photodiode with a graphene phototransistor," *Nat. Commun.*, vol. 7, 2016.

[3] K. S. Novoselov, V. Fal, L. Colombo, P. Gellert, M. Schwab, K. Kim *et al.*, "A roadmap for graphene," *Nature*, vol. 490, no. 7419, pp. 192–200, 2012.

[4] D. V. Talapin, J.-S. Lee, M. V. Kovalenko, and E. V. Shevchenko, "Prospects of colloidal nanocrystals for electronic and optoelectronic applications," *Chem. Rev.*, vol. 110, no. 1, pp. 389–458, 2009.

[5] N. Kitazawa, Y. Watanabe, and Y. Nakamura, "Optical properties of CH3NH3PbX3 (X= halogen) and their mixed-halide crystals," *J. Mater. Sci.*, vol. 37, no. 17, pp. 3585–3587, 2002.

[6] F. Koppens, T. Mueller, P. Avouris, A. Ferrari, M. Vitiello, and M. Polini, "Photodetectors based on graphene, other two-dimensional materials and hybrid systems," *Nat. Nanotechnol.*, vol. 9, no. 10, pp. 780–793, 2014.

[7] G. Konstantatos, M. Badioli, L. Gaudreau, J. Osmond, M. Bernechea, F. P. G. De Arquer, F. Gatti, and F. H. Koppens, "Hybrid graphene-quantum dot phototransistors with ultrahigh gain," *Nat. Nanotechnol.*, vol. 7, no. 6, pp. 363–368, 2012.

[8] Y. Lee, J. Kwon, E. Hwang, C.-H. Ra, W. J. Yoo, J.-H. Ahn, J. H. Park, and J. H. Cho, "High-performance perovskite–graphene hybrid photodetector," *Adv. Mater.*, vol. 27, no. 1, pp. 41–46, 2015.

[9] S. H. Yu, Y. Lee, S. K. Jang, J. Kang, J. Jeon, C. Lee, J. Y. Lee, H. Kim, E. Hwang, S. Lee *et al.*, "Dye-sensitized MoS2 photodetector with enhanced spectral photoresponse," *ACS Nano*, vol. 8, no. 8, pp. 8285–8291, 2014.

[10] K. Roy, M. Padmanabhan, S. Goswami, T. P. Sai, G. Ramalingam, S. Raghavan, and A. Ghosh, "Graphene-MoS2 hybrid structures for multifunctional photoresponsive memory devices," *Nat. Nanotechnol.*, vol. 8, no. 11, pp. 826–830, 2013.

[11] M. R. Pinto, k. smith, M. A. Alam, S. Clark, X. Wang, G. Klimeck, and D. Vasileska, "Padre," Jan 2006. [Online]. Available: https://nanohub.org/resources/padre

[12] E. Davis, "Electronic and structural properties of amorphous semiconductors," *Academic Press, NY*, 1973.

[13] K. S. Jeong, J. Tang, H. Liu, J. Kim, A. W. Schaefer, K. Kemp, L. Levina, X. Wang, S. Hoogland, R. Debnath *et al.*, "Enhanced mobility-lifetime products in PbS colloidal quantum dot photovoltaics," *ACS Nano*, vol. 6, no. 1, pp. 89–99, 2011.

[14] B. K. Sarker, I. Childres, E. Cazalas, I. Jovanovic, and Y. P. Chen, "Gate-tunable and high responsivity graphene phototransistors on undoped semiconductor substrates," *arXiv preprint arXiv:1409.5725*, 2014.